Intense and tunable upconversion luminescence of Er^{3+}/Yb^{3+} co-doped oxy-fluoride phosphors

QUN HAN[a,c,*], HUILING SONG[a,c], FANGCHAO LIU[a,b], XIAOYUN TANG[a,c], YAOFEI CHEN[a,c], WENCHUAN YAN[a,c], TIEGEN LIU[a,c]

[a]*College of Precision Instruments and Optoelectronic Engineering, Tianjin University Tianjin, 300072, China*
[b]*China North Vehicle Research Institute, Beijing, 100072, China*
[c]*Key Laboratory of Opto-Electronics Information Technology of the Ministry of Education, Tianjin University, Tianjin, 300072, China*

The synthesis and up-conversion (UC) luminescence properties of Er^{3+}/Yb^{3+} co-doped oxy-fluoride phosphors are reported in this paper. The phosphors were synthesized by the high-temperature melting method and phase identified by X-ray diffraction. Intense red and green emissions were observed under 980 nm excitation which were ascribed to the $^4F_{9/2}\rightarrow{}^4I_{15/2}$ and $^4H_{11/2}$, $^4S_{3/2}\rightarrow{}^4I_{15/2}$ transitions of Er^{3+}, respectively. Mechanisms of UC by two and three-photon and energy transfer process were interpreted and explained. The color coordinates were measured and the tunable UC luminescence was analyzed. The CIE diagram shows that the samples with different Yb^{3+} ion concentrations exhibit different colors.

(Received May 21, 2017; accepted April 5, 2018)

Keywords: Tunable up-conversion, Er^{3+}/Yb^{3+} co-doped, Energy transfer

1. Introduction

Upconversion (UC) is a multi-photon spectroscopic process that converts two or more lower energy (longer wavelength) photons into one higher energy (shorter wavelength) photon [1]. In the last few decades, increasing attention has been paid to the study of rare-earth doped UC luminescence materials owing to their promising applications in various technologies, such as white LEDs [2], power and coherent laser sources [3], three-dimensional displays [4,5], bio-imaging [6,7] and sensors [8-10] etc. Especially, UC in several trivalent rare-earth doped materials has been found to be very efficient [11-14]. In such materials, the UC is mainly happened through multi-photon processes such as the excited state absorption and cross-relaxation between adjacent levels. Co-doping with Yb^{3+} as sensitizer further increases the efficiency of the UC process through donor-acceptor process in rare earths like Tm^{3+}, Ho^{3+}, Er^{3+} ions [15-17]. Because of the large spectral overlap between the Yb^{3+} emission ($^2F_{5/2}\rightarrow{}^2F_{7/2}$) and the Er^{3+} absorption ($^4I_{15/2}\rightarrow{}^4I_{11/2}$), the resonant energy transfer (ET) from Yb^{3+} to Er^{3+} is very efficient. This makes erbium the most popular and efficient one among the lanthanide ions to generate visible and infrared fluorescence.

A good host for UC phosphors should have a phonon energy as low as possible in order to achieve high-efficiency radiative emissions, in which the competitive phonon-assisted non-radiative deactivation could be inhibited to the utmost. Oxy-fluoride has a low phonon matrices, good chemical stability, and low toxicity. It can also be easily mass produced at a low cost. These make it an ideal hosts for UC phosphors [18-21]. Fluorides materials play an important role in forming the oxy-fluoride phase of the samples in the melt quenching method. Because of their high solubility for both of the sensitizer and activator rare earth ions and high transparency in the near UV to middle infrared range, CaF_2, PbF_2, and AlF_3 crystals are commonly used [18].

In this letter, Er^{3+}/Yb^{3+} co-doped CaF_2-PbF_2-AlF_3 phosphors with various concentrations of Yb^{3+} were synthesized by the melt quenching method. The X-ray diffraction (XRD) and the UC emission spectra were measured to analyze their structural and spectral properties. Intense and tunable cooperative UC emission was observed when the samples was excited by a continuous-wave (CW) laser at 980 nm. The dependence of the emission property on the pump-power and Yb^{3+} concentration were investigated. Explanations based on the structure, sensitizer concentration dependency, and energy transfer mechanisms about the spectroscopic properties of the material were also discussed.

2. Experimental

2.1. Sample preparation

The precursor glasses codoped with ytterbium and erbium were prepared by the high-temperature melting method. High-purity chemicals AlF_3, PbF_2, CaF_2, Er_2O_3

(99.99%), Yb_2O_3 (99.99%) were used for batch melting. The composition of the glass was AlF_3-PbF_2-CaF_2-2.4Er_2O_3-xYb_2O_3 (x=4.8, 9.6, 14.4, 19.2, 24, 28.8). The mixture was filled into a corundum crucible and heated in an electric arc furnace. Temperature was increased with a step of 10℃/min to 700℃ and then with a step of 5℃/min to the highest target temperature 1200℃ and kept in there for 40 min. Then the melts were annealed at 300℃ for 12 h to avoid the thermal strains otherwise would occur during a sudden quenching. Lastly, the compound was milled to powder by planetary ball-milling with a rotation speed of 400 rpm for 60 min and an interruption time for 10 min. Agate balls with a diameter of ~10 mm were used in the milling process.

2.2. Sample characterization

X-ray diffraction (XRD) patterns were measured for phase identification of the powders by using a rotating anode X-ray diffractometer (D/MAX-2500) under Cu K_α radiation (λ=0.154 nm), with a scanning rate of 10°/min in the 2θ range from 10° to 80°. The slits of X-ray diffractometer are 1.00 deg (DivSlit), 1.00 deg (SctSlit) and 0.20 mm (RecSlit). The UC spectra were measured with a Hitachi F-4600 fluorescence spectrophotometer with a 980 nm CW laser as the excitation source. All the above measurements were carried out at a room temperature of ~25℃.

3. Results and discussion

3.1. Phase and structure analysis

XRD patterns of the Er^{3+}/Yb^{3+} co-doped oxy-fluoride phosphors prepared by the high-temperature melting method are shown in Fig. 1. The concentration ratio of Er/Yb of the sample was 1:4. From Fig. 1 three crystal phases can be identified, i.e. (a) $CaPb(OH)_6$, (b) $Ca_2PbAl(F,OH)_9$, and (c) $Ca_2Pb_2O_5(OH)_2$, which are marked by triangle, square, and circle, as shown in Fig. 1(a)-(c), respectively.

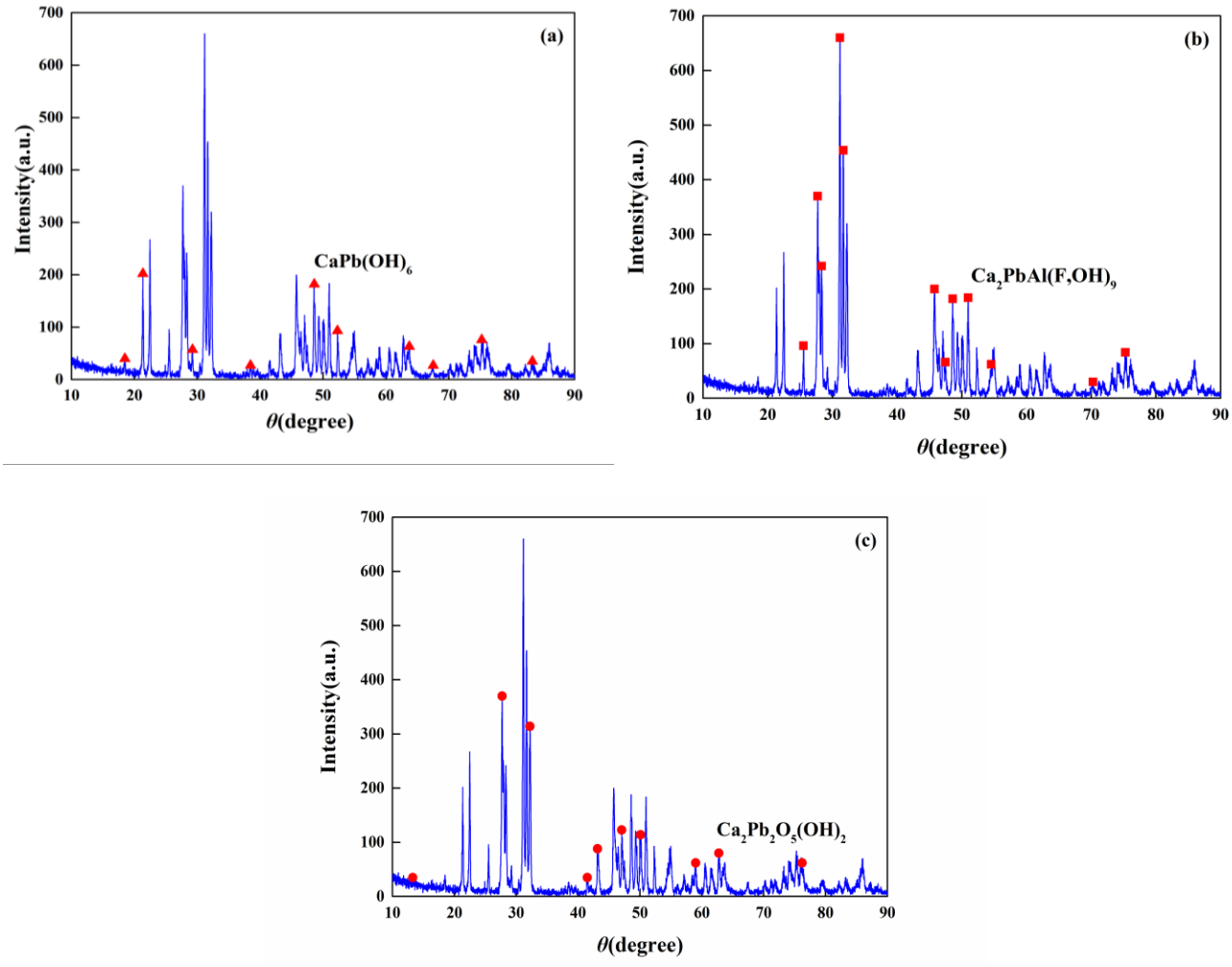

Fig. 1. X-ray diffraction patterns of Er^{3+}/Yb^{3+} co-doped oxy-fluoride powders sintered at 1200 ℃ and the reference patterns marked corresponding to the (a) $CaPb(OH)_6$ (b) Sample powders (c) $Ca_2Pb_2O_5(OH)_2$ (ICSD database)

3.2. Up-conversion emission under 980 nm excitation

In order to analyze the dependence of the relative intensity of the red and green emission on the Yb^{3+} concentrations, spectra of the six samples excited at 100 mW were compared in Fig. 2. As shown in Fig. 2, the emission intensity of the green emission band first increased then decreased with the increase of Yb^{3+} concentration. This is caused by the interaction between the neighboring Yb^{3+} and Er^{3+} ions and the concentration quenching effect of Yb^{3+} ions [22]. Apparently, for the green emission (523 nm and 541 nm, corresponding to the $^2H_{11/2}\rightarrow{}^4I_{15/2}$ and $^4S_{3/2}\rightarrow{}^4I_{15/2}$ transitions of Er^{3+} ion[23]) the best Yb^{3+} concentration was x=9.6 among the samples.

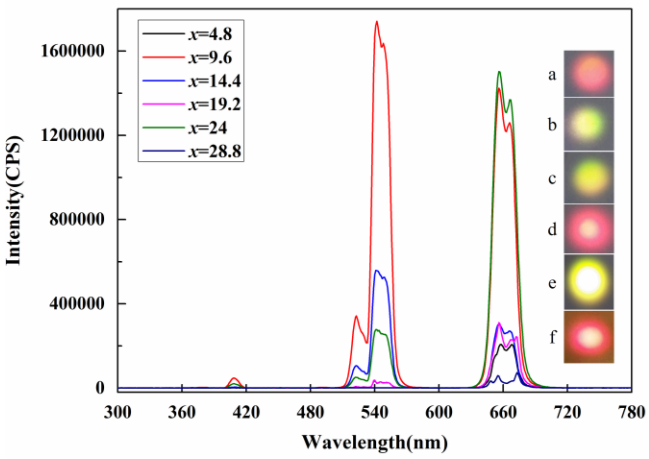

Fig. 2. Up-conversion spectra of the samples with different Yb^{3+} ions doping concentration (a-f corresponding to x=4.8-28.8) excited at 980 nm upon 100 mw, the inset shows the emission photographs of samples with different Yb^{3+} concentrations excited upon 20 mW (a-f corresponding to x=4.8-28.8, respectively)

As for the red emission band (665 nm corresponding to the $^4F_{9/2}\rightarrow{}^4I_{15/2}$ transition [24]), there exits two peaks when x=9.6 and 24. The intensity of the latter is slightly stronger than that of the former. The first peak is caused by the concentration quenching effect induced by the shortening distance between the Er^{3+} and Yb^{3+} ions with the increase of the Yb^{3+} concentration. The second peak emission is mainly attributed to the energy back transfer (EBT) process. As increasing Yb^{3+} concentration, the enhanced rate of EBT ($Er^{3+}(^4S_{3/2})+Yb^{3+}(^2F_{7/2})\rightarrow Er^{3+}(^4I_{13/2})+Yb^{3+}(^2F_{5/2})$) and $^4I_{13/2}\rightarrow{}^4F_{9/2}$ transition results in higher red emission [25]. Because the intensities of the green and red emissions are tunable with the Yb^{3+} concentration, the samples glow with different colors due to color mixing. The UC fluorescence of these samples is very bright and can be easily observed with the naked eyes. To relieve saturation of the CCD camera, pictures of the samples were taken at the lowest power of the excitation laser ~20 mW and is shown in the inset of Fig. 2, where *a-f* corresponding to x=4.8, 9.6, 14.4, 19.2, 24 and 28.8 respectively.

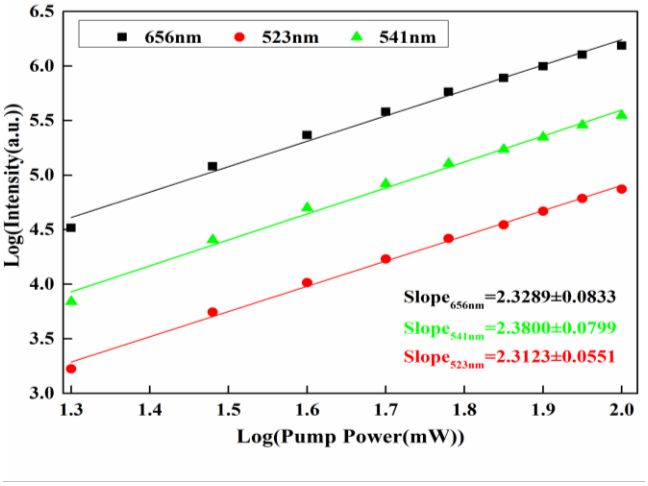

Fig. 3. The pump power dependence of the red and green UC emissions in Er^{3+}/Yb^{3+} co-doped oxy-fluoride phosphors under 980 nm excitation

It is well known that the UC intensity (I) depends on the pump power (P) following the relationship $I \propto P^n$ [26], where n is the number of pumping photons absorbed by the rare earth ions at the ground level to transit to the upper emitting level. In order to investigate the UC mechanism of the Er^{3+}/Yb^{3+} co-doped Sample powders series, the dependence of the intensity of the two bands on the pump power was measured. Fig. 3 shows the intensities of the 523, 541 and 656 nm emission asa function of the pump power in a log-log scale diagram. The calculated slopes are 2.38 for green ($^4S_{3/2}\rightarrow{}^4I_{15/2}$) and 2.32 for red ($^4F_{9/2}\rightarrow{}^4I_{15/2}$) emissions, respectively. The slopes are noticeably larger than 2, indicating more than two photons are involved to generate one UC photon. This implies that the red and green emissions may both come from a two-photon and three-photon process.

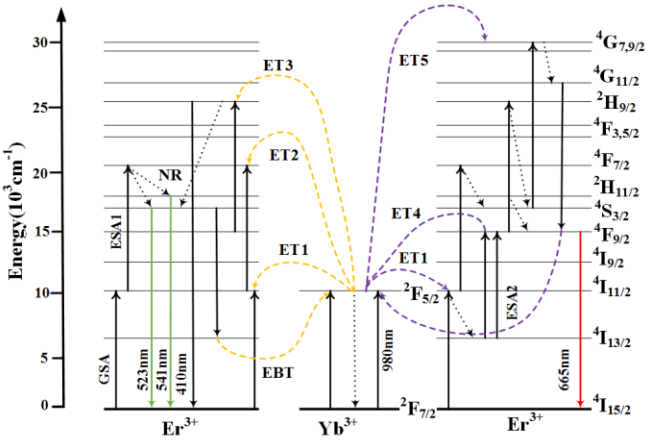

Fig. 4. Energy level diagram of the Er^{3+}, Yb^{3+} ions and the proposed UC mechanisms in Er^{3+}/Yb^{3+} co-doped sample phosphors

Usually, the UC emissions of Er^{3+} can be explained by several well-known mechanisms such as the excited-state absorption (ESA), the energy-transfer up-conversion (ETU), and the photon avalanche (PA) [27,28]. To better understand the populating process of the emitting levels and the radiative transitions of the green and red UC luminescence, the energy diagram and the UC mechanisms of the Er^{3+}/Yb^{3+} co-doped sample powders are schematically shown in Fig. 4. Under 980 nm excitation, an Yb^{3+} ion absorbs an infrared photon and transits from the ground level $^2F_{7/2}$ to the excited level $^2F_{5/2}$ and an Er^{3+} ion can be excited from the ground level $^4I_{15/2}$ to the excited level $^4I_{11/2}$ through the ground state absorption (GSA): $Er^{3+}(^4I_{15/2})$ + a phonon (980 nm) → $Er^{3+}(^4I_{11/2})$ or the Yb→Er energy transfer (ET1): $Er^{3+}(^4I_{15/2}) + Yb^{3+}(^2F_{5/2})$ → $Er^{3+}(^4I_{11/2})$ +$Yb^{3+}(^2F_{7/2})$. For the above mentioned processes, the ET1 process plays a dominant role because the absorption cross section of the $^2F_{7/2}$ → $^2F_{5/2}$ transition of Yb^{3+} (~34.07 × 10^{-19} cm^2) is about eight times higher than that of the $^4I_{15/2}$ →$^4I_{11/2}$ transition of Er^{3+} (~4.3 × 10^{-19} cm^2) [29]. Then the $^4F_{7/2}$ level of the Er^{3+} is populated via ET2: $Er^{3+}(^4I_{11/2})$ +$Yb^{3+}(^2F_{5/2})$ → $Er^{3+}(^4F_{7/2})$ + $Yb^{3+}(^2F_{7/2})$ and the excited state absorption (ESA1): $Er^{3+}(^4I_{11/2})$ + a pump phonon (980 nm) →$Er^{3+}(^4F_{7/2})$. The upper levels of the green emission, i.e., $^2H_{11/2}$ and $^4S_{3/2}$, are populated by a rapid non-radiative relaxation (NR) from the $^4F_{7/2}$ level due to the small energy gap between these levels. Finally, the $^2H_{11/2}$ → $^4I_{15/2}$ and $^4S_{3/2}$ → $^4I_{15/2}$ transitions of Er^{3+} ions produce the 523 nm and 541 nm green emissions, respectively. As mentioned before, in Fig. 3, the slop of 2.38 implies that a three-photon process is also involved in the green UC luminescence, which can be described as: $Er^{3+}(^4F_{9/2})$ + $Yb^{3+}(^4F_{5/2})$ → $Er^{3+}(^2H_{9/2})$ + $Yb^{3+}(^2F_{7/2})$ (ET3) followed by $Er^{3+}(^2H_{9/2})$ → $Er^{3+}(^2H_{11/2},^4S_{3/2})$ (NR) [30]. The weak blue emission at 410nm in Fig. 2 arises from the $^2H_{9/2}$ → $^4I_{15/2}$ transition. For the red emission ($^4F_{9/2}$ →$^4I_{15/2}$), the population of the emitting level $^4F_{9/2}$ involves the following possible processes: $Er^{3+}(^4I_{13/2})$ + a pump phonon (980 nm) →$Er^{3+}(^4F_{9/2})$ (ESA2), where the $^4I_{13/2}$ level is populated by a NR from the $^4I_{11/2}$ level, and $Er^{3+}(^4I_{13/2})$ + $Yb^{3+}(^2F_{5/2})$ → $Er^{3+}(^4F_{9/2})$ + $Yb^{3+}(^2F_{7/2})$ (ET4) and a NR from $^4S_{3/2}$ to $^4F_{9/2}$. Since the slop of the red emission 2.32 is also larger than 2, a third energy transfer: $Er^{3+}(^4S_{3/2})$ + $Yb^{3+}(^2F_{5/2})$→$Er^{3+}(^4G_{7/2})$ + $Yb^{3+}(^2F_{7/2})$ (ET5) is also involved. After reaching the $^4G_{7/2}$ level, the Er^{3+} decays to the $^4G_{11/2}$ level and then undergoes a cooperative decay to the red emitting $^4F_{9/2}$ level.

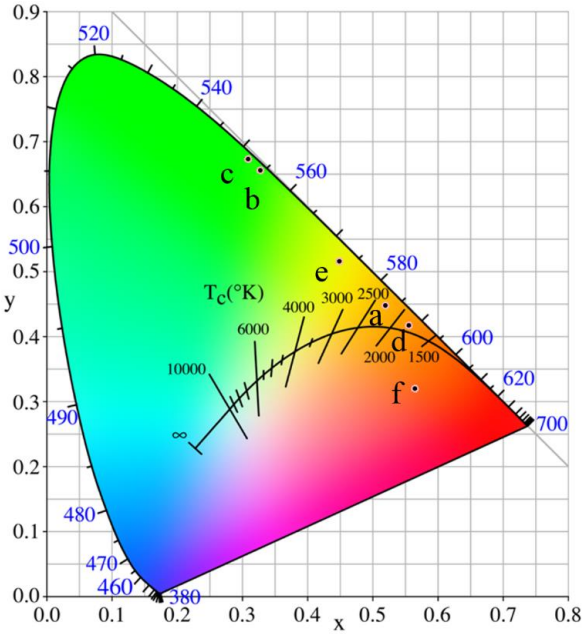

Fig. 5. CIE color coordinate diagram shows the chromatically point for luminescence of the samples with the changing of Yb^{3+} ions doping concentration (x=4.8, 9.6, 14.4, 19.2, 24, 28.8)

Actually, Yb^{3+} ion is used as a sensitizer for the ET from Yb^{3+} to Er^{3+}. The enhancement of the UC emission intensities with the increase of the Yb^{3+} concentration can be explained by the interionic distance change between the Er^{3+} and Yb^{3+} ions. With the increase of Yb^{3+} concentration, the average distance between the Er^{3+} and Yb^{3+} ion decreases, which automatically enhances the energy transfer process from Yb^{3+} to Er^{3+} ions. However, if the concentration of the Yb^{3+} ions is so high as the concentration quenching effect becoming dominant, then the UC emission intensities decrease with the further increase the Yb^{3+} concentration. So by controlling the doping concentration of Yb^{3+} we can change the interionic distance between the Er^{3+} and Yb^{3+} ions. This, in turn, changes the degree of the concentration quenching of Yb^{3+} ions, and finally changes the red and green UC emissions (i.e., fluorescence color, as shown in Fig. 2) of the phosphor. In order to show the trace of the color variation, the Commission International de L' Eclairage (CIE) color coordinates calculated from the emission spectra of the samples with different Yb^{3+} concentration is shown in Fig. 5. The color of the samples can vary in a wide range covering green (0.309, 0.674), yellow (0.449, 0.516), orange (0.556, 0.418), and reddish orange (0.564, 0.321).

Table. 1. X and Y values of chromaticity diagram of the samples with the changing of Yb^{3+} ions doping concentration (x=4.8, 9.6, 14.4, 19.2, 24, 28.8)

sample	a	b	c	d	e	f
X value	0.519	0.326	0.309	0.556	0.449	0.564
Y value	0.451	0.656	0.674	0.418	0.516	0.321

4. Conclusions

Er^{3+}/Yb^{3+} co-doped oxy-fluoride phosphors with six different Yb^{3+} concentrations were prepared by the high–temperature melting method. Under the excitation of a 980 nm CW laser, the UC luminescence spectra of the samples were measured and analyzed. Intense luminescence was observed. The color of the emission can be turned in a wide range in the visible spectrum covering green, yellow, orange, and reddish orange by adjusting the concentration of Yb^{3+}. The underlying mechanism was also discussed based on the energy level diagram of the Er/Yb codoped system. The intense and tunable UC luminescence of this kind of material is attractive for many applications in fields such as lighting, color displaying, and so on.

Acknowledgements

This work was supported by the Natural Science Foundation of Tianjin [grant number 13JCYBJC16100]; the National Natural Science Foundation of China [grant number 61107035]; the National Key Scientific Instrument and Equipment Development Project of China [grant number 2013YQ03091502] and the National Basic Research Program of China [grant number 2014CB340104].

References

[1] François Auzel, Chem. Rev. **104**, 139 (2004).
[2] Anthuvan John Peter, I. B. Shameem Banu, Optoelectron. Adv. Mat. **10**(7-8), 472 (2016).
[3] Subrata Das, A. Amarnath Reddy, G. Vijaya Prakash, Chem. Phys. Lett. **504**, 206 (2011).
[4] G Seeta Rama Raju, Jin Young Park, Hong Chae Jung, E. Pavitra, Byung Kee Moon, Jung Hyun Jeong, Jae Su Yu, Jung Hwan Kim, Haeyoung Choi, J. Alloys Compd. **509**, 7537 (2011).
[5] Y. Dwivedi, Kavita Mishra, S. B. Rai, J. Alloys Compd. **572**, 90 (2013).
[6] Jun Ho Chung, Jeong Ho Ryu, Jong Won Eun, Jeong Hoon Lee, Sang Yeop Lee, Tae Hyung Heo, Bong Geun Choi, Kwang Bo Shim, J. Alloys Compd. **522**, 30 (2012).
[7] Xin Yang, Lufang Guo, Yuanhui Zuo, Jing Li, Hongchen Mou, Optoelectron. Adv. Mat. **10**(7-8), 467 (2016).
[8] J. Suresh Kumar, K. Pavani, M. P. F. Graça, M. J. Soares, J. Alloys Compd. **617**, 108 (2014).
[9] B. S. Cao, Y. Y. He, L. Zhang, B. Dong, J. Lumin. **135**, 128 (2013).
[10] Jikai Yang, Siguo Xiao, Jianwen Ding, Xiaoliang Yang, Xiangfu Wang, J. Alloys Compd. **474**, 424 (2009).
[11] Qiwei Zhang, Haiqin Sun, Xusheng Wang, Tao Zhang, Mater. Lett. **117**, 283 (2014).
[12] E. Polikarpov, D. Catalini, A. Padmaperuma, P. Das, T. Lemmon, B. Arey, C. A. Fernandez, Opt. Mater. **46**, 614 (2015).
[13] Jilin Zhang, Weilu Zhang, Zhongxian Qiu, Wenli Zhou, Liping Yu, Zhiqiang Li, Shixun Lian, J. Alloys Compd. **646**, 315 (2015).
[14] Wei Xu, Hua Zhao, Zhiguo Zhang, Wenwu Cao, Sensors and Actuators B: Chemical. **178**, 520 (2013).
15] Tomasz Grzyb, Sangeetha Balabhadra, Dominika Przybylska, Mariusz Węcławiak, J. Alloys Compd. **649**, 606 (2015).
[16] M. Seshadri, L. C. Barbosa, C. M. B. Cordeiro, M. Radha, F. A. Sigoli, Y. C. Ratnakaram, J. Lumin. **166**, 8 (2015).
[17] J. J. Leal, R. Narro-García, H. Desirena, J. D. Marconi, E. Rodríguez, K. Linganna, E. De la Rosa, J. Lumin. **162**, 72 (2015).
[18] Weirong Wang, Huiping Gao, Yanli Mao, J. Alloys Compd. **648**, 75 (2015).
[19] Jihong Zhang, Jong Heo, J. Non-Cryst. Solids **383**, 188 (2014).
[20] M. Secu, C. E. Secu, J. Non-Cryst. Solids **426**, 78 (2015).
[21] G A. Kumar, M. Pokhrel, A. Martinez, R. C. Dennis, I. L. Villegas, D. K. Sardar, J. Alloys Compd. **513**, 559 (2012).
[22] Yuanyuan Tian, Yue Tian, Ping Huang, Lei Wang, Qiufeng Shi, Cai'e Cui, Chem. Eng. J. **297**, 26 (2016).
[23] Fiorenzo Vetrone, John-Christopher Boyer, John A. Capobianco, Adolfo Speghini, Marco Bettinelli, J. Appl. Phys. **96**, 661 (2004).
[24] Liansheng Shi, Qinyun Shen, Zhaozhong Qiu, J. Lumin. **148**, 94 (2014).
[25] Do Rim Kim, Sung Wook Park, Byung Kee Moon, Sung Heum Park, Jung Hyun Jeong, Haeyoung Choi, Jung Hwan Kim, RSC Advances **7**, 1464 (2017).
[26] M. Pollnau, D. R. Gamelin, S. R. Lüthi, H. U. Güdel, M. P. Hehlen, Phys Rev B **61**, 3337 (2000).
[27] M. Jiménez de Castro, J. M. Fernández Navarro, Appl. Phys. B **106**, 669 (2012).
[28] P. V. dos Santos, M. V. D. Vermelho, E. A. Gouveia, M. T. de Araujo, A. S. Gouveia-Neto, F. C. Cassanjes, S. J. L. Ribeiro, Y. Messaddeq, J. Alloys Compd. **344**, 304 (2002).
[29] Hyeon Mi Noh, Hyun Kyoung Yang, Byung Kee Moon, Byung Chun Choi, Jung Hyun Jeong, Haeyoung Choi, Jung Hwan Kim, Jpn. J. Appl. Phys. **52**, 01AM02 (2013).
[30] Guanying Chen, Gabriel Somesfalean, Yan Liu, Zhiguo Zhang, Qiu Sun, Fuping Wang, Phys. Rev. B **75**, 195204 (2007).

*Corresponding author: hanqun@tju.edu.cn